

MULTIPOINT INVERSE DESIGN FOR TRANSONIC, SLOTTED, NATURAL-LAMINAR-FLOW WINGS

Andrew Heletkanycz[1], Christopher J. Axten[1] & James G. Coder[1]

[1]The Pennsylvania State University, University Park, PA 16801, United States

Abstract

A method is presented for the multipoint, three-dimensional inverse design of slotted, natural-laminar-flow wings. It is based on pressure-curvature relation used by CDISC, but it is augmented using the approach of Eppler. Wing sections are subdivided into multiple segments for which the target pressures come from different design points. The curvature update equation is expressed as a Newton-Raphson problem that solves for surface displacements along the normal vector at each grid node. Geometric constraints are enforced by overconstraining the system of equations with large weighting factors and solving by least squares. Representative results from various airfoil and wing cases, both single- and multielement, are shown to demonstrate the efficacy of the method.

Keywords: Aerodynamics, Transition, NLF, Inverse Design

1. Introduction

Maintaining significant runs of flow in the laminar boundary layer reduces skin friction drag, therefore increasing aircraft efficiency. Various conceptual designs, such as the MIT/Aurora Double Bubble [1], Boeing Transonic Truss-Braced Wing [2], and the newer Boeing/Aurora AACES concept [3], acknowledge these potential efficiency gains through extended regions of laminar flow on the main wing. For these gains to be realized, mechanisms of boundary layer transition need to be controlled.

Multiple techniques have been developed to increase the amount of laminar flow present on aircraft, and typically fall under two catagories, active and passive flow control. Laminar Flow Control (LFC) techniques use suction to laminarize and/or maintain a laminar boundary layer. Hybrid Laminar Flow Control (HLFC) uses suction around the leading edge region of the airfoil to laminarize the boundary layer and a favorable pressure gradient to retain the laminar boundary layer for as long as possible [4]. These methods are categorized as “active flow control" methods. While shown to be effective, active flow control requires additional hardware which adds complexity and additional costs to an aircraft. Natural Laminar Flow (NLF) airfoils aim to promote a laminar boundary layer purely through the design of the pressure distribution. These airfoils utilize long extents of favorable pressure gradients, which act to suppress Tollmien-Schlichting instabilities in the boundary layer, delaying transition

Modern transonic aircraft utilize wing sweep to increase cruise speeds without incurring outsized wave drag penalties. When the NLF airfoil design methodology is applied to swept wings, it promotes the rapid growth of crossflow instabilities. Crossflow arises from a misalignment between the direction of flow and the direction in which the pressure force acts [5]. On swept wings, pressure isobars are approximately parallel to the leading edge of the wing, while the flow arrives at an angle relative to the leading edge. The resulting spanwise boundary layer velocity profile has an inflection point, which is a sufficient condition for an instability to arise and cause transition in a laminar boundary

layer.

Crossflow attenuated natural laminar flow (CATNLF) airfoils aim to address the aforementioned crossflow instabilities [6]. Under the CATNLF strategy, the flow is rapidly accelerated over the first few percent of the chord, inducing a strong favorable pressure gradient. Before the crossflow instability can go critical, the pressure gradient is switched to be near-neutral and allow the crossflow to damp while the TS instabilities grow slowly. Another NLF design strategy that has gained traction is the use of slotted, natural-laminar-flow airfoils [7]. Several studies have been conducted, such as with the S207 airfoil designed for low-sweep transonic, truss-braced wing aircraft [8, 9]. A theoretical study for SNLF on higher-sweep aircraft was conducted by Hiller et al. [10], but this work is still nascent.

To realize the benefits of the NLF airfoil design, precise control during the design of the airfoil pressure distribution is required. Over the decades, multiple methods for inverse airfoil design have been develop and applied. One of the first methods be developed were conformal mapping methods such as those developed by Joukowsky and von Mises. These methods are analytical, making them easy to evaluate. However, since these are potential flow methods they do not provide estimates for drag or account for compressibility effects. Eppler developed a conformal mapping method allowing for multipoint inverse design. This was done by specifying portions of the airfoil surface where the c_p distribution is to be constant for a prescribed angle of attack [11]. A boundary layer solver was then incorporated to account for viscous effects, resulting in the PROFIL inverse design code. Seilig extended Eppler's method by allowing for the prescription of a c_p distribution as a function of arc length instead of specifying a constant c_p [12]. Coupling a boundary layer solver to potential flow methods provides a drag estimate, but still does not allow for inverse design in the compressible regime. The MSES code by Drela, couples the Euler equations in the free stream with a boundary layer equations at the surface of an airfoil [13]. This code also features inverse design capabilities; however, the c_p distribution inverse design mode only allows for design at one flight condition. It also lacks the ability to model three-dimensional flow behaviors, such as the impact of sweep and taper on surface pressures or the presence of crossflow in the boundary layer.

To accurately model three dimensional effects, a solver with three dimensional and inherent inverse design capabilities must be used. Alternatively, an external inverse design method may be coupled to a three dimensional solver, such as the Constrained Direct Iterative Surface Curvature (CDISC) method. This method leverages a simple relationship between change in curvature and the change in pressure for inverse design, utilizing an external solver to provide flow field data [14]. This method has been extensively used for airfoil and three dimensional inverse design [15, 16]. However, the method as published in the literature lacks a dedicated capability for multipoint, inverse design. Therefore, developing a tool that leverages the underlying mathematical simplicity of the CDISC method while allowing the for multipoint design is the primary objective of this work.

2. Methodology and Implementation

2.1 Governing Equations

The fundamental relations used in this method are those given by Campbell and Smith in their CDISC method, which provides a relationship between the change in curvature, κ, and the resulting change in c_p [14]. For subsonic flows, this relationship may be expressed as

$$d\kappa = A\left(1+\kappa^2\right)^B dc_p \tag{1}$$

where B is a constant typically set at 0.4 and Δc_p is the difference between the target pressure and the current pressure at that point on an airfoil.

If the local Mach number becomes sufficiently large, the behavior of the flow becomes locally hyperbolic and the curvature relation no longer holds. This characteristic change hinders the convergence of Eq. 1. To improve convergence in regions where the local Mach number exceeds 1.2, the following relation is used:

$$d\kappa = A \frac{\frac{d}{dx}(dC_p)}{1 + \left(\frac{dy}{dx}\right)^2} \tag{2}$$

where x and y represent the ordinate and abscissa of a point on the surface of an airfoil, and A may be set to a constant value such as 0.05. For this work, the supersonic relationship was not used as the inverse design converged adequately fast utilizing the subsonic relationship alone. Since the equations remained entirely dependent on curvature, a smoothing step for the perturbations was not required.

The initial implementation, by Campbell and Smith, approximates the required change in curvature with the change in the the local second derivative of the airfoil surface. Instead, this work employs a linear system of equations to solve for the normal surface perturbations required to obtain a specific curvature. A Jacobian is numerically computed which contains the sensitivities of the change in curvature to the normal perturbations of the surface. The resulting matrix, M, is a tridiagonal matrix, as the local curvature requires three points to be computed. This results in the following expression,

$$\mathbf{M} \frac{\partial \kappa}{\partial \mathbf{n}} \Delta \mathbf{n} = \Delta \mathbf{c_p} \tag{3}$$

and when combined with Eqs. 1 and/or 2, yields the relationship used in this work.

The matrix $\frac{\partial \kappa}{\partial \mathbf{n}}$ has a tridiagonal structure as a result of the use of the Menger three-point curvature definition, whereas $\mathbf{M}^{-1}$ is diagonal when the subsonic relation is used and tridiagonal when the supersonic relation is used. Geometric constraints are imposed by appending the equation set, creating an overconstrained system that is solved in a least squares sense. While one may define Lagrange multipliers, the current implementation uses weighting factors on the constraint equations to ensure that they are satisfied, even if the final pressure target cannot be achieved. Numerical experimentation found this to give geometry updates that are more reliably smooth than projecting the update vector onto a permissible space.

2.2 Pressure Specification

The multipoint extension to the CDISC method is inspired by Eppler [11] and, later, Selig [12] where different sections of the surface of an airfoil are designed at different flight conditions. Their approach was built on conformal mapping where the surface could be subdivided into angular arc limits. A desired functional c_p behavior (e.g., constant) and the absolute angle attack at which it is achieved is specified for each segment. Each segment is allowed to have its own unique angle of attack, so the behavior for multiple design points may be handled simultaneously. The angle-of-attack distribution also need not be continuous, as the constraints of conformal mapping ensures a continuous pressure distribution.

Transonic, SNLF airfoils are not conducive to conformal-mapping design strategies, so an alternative method of specification must be used. While many tools, such as MSES [13], specify based on x/c, this reduces the control around the leading edge. Instead, the present work specifies the pressure distribution based on normalized arc length s/s_{total} around the airfoil. The overall specification strategy is illustrated in the example in Fig. 1.

The desired pressure distributions may be selected in multiple different ways, each with their own shortcomings. For instance, there is no guarantee that the specified pressure distribution is attainable by a single airfoil. It is therefore advised that specified pressure distributions be not too different from the seed airfoil. Alternatively, one may specify one or more segments as having a desired functional behavior (such as the Eppler method [11], in which case it is suggested that the average value of c_p in the region be matched.

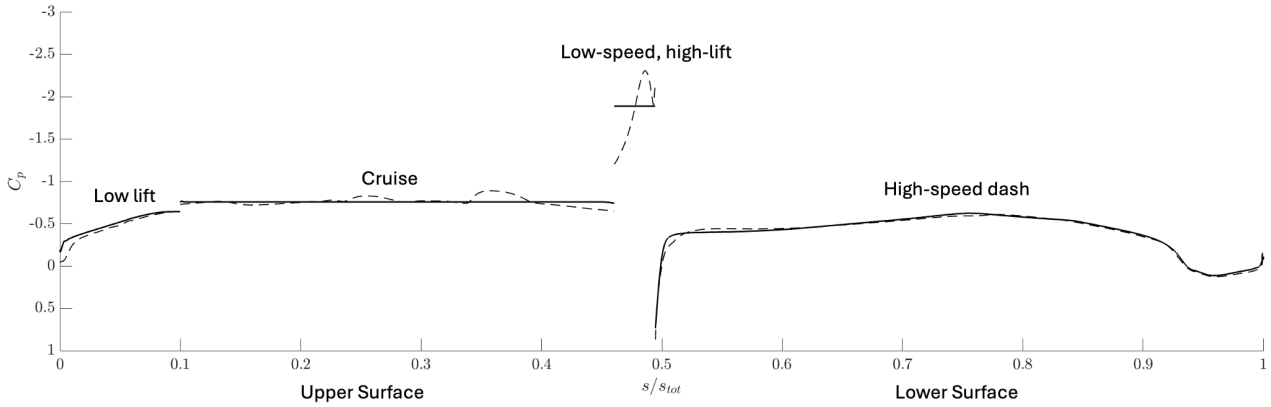


Figure 1 – Example multipoint inverse design specification (dashed: initial; solid: target)

For three dimensional applications, such as wings, the two-dimensional method is applied to multiple spanwise sections. The regions between the updated airfoil sections are then lofted to produce a new wing surface.

2.3 Geometric Constraints

2.3.1 Fixed Regions

Not every airfoil constraint is aerodynamic, as some are purely geometric. If the airfoil has a finite thickness trailing edge or a region with a defined clearance for a flap or a control surface, a constraint to prevent modification in those regions must be used. This is done by imposing that $\Delta n = 0$ for each point in that region, which overconstrains in the system of linear equations. An overconstrained linear system can be solved with the use of a pseudo inverse, which provides the least squares solution. To ensure the constraints are reflected in the solution, a weight of 1×10^8 is applied to each constraint in the matrix.

2.3.2 Leading-Edge Hold

Since Eq. 1 is not valid at a stagnation point, another constraint is needed to prevent excessive changes in curvature. The following constraint,

$$\sum_{1}^{N} D\Delta n_j = 0, \tag{4}$$

is usually applied to airfoil points that reside before $5\%\ \frac{x}{c}$, but this may vary depending on the airfoil and design case. The coefficient D ranges from 1 to $1{,}000$, which is also case dependent. As the coefficient D is increased, the coefficient B needs to decrease to prevent the solution from diverging.

2.3.3 Arc-Length Constraint

Drift of the leading edge can alternatively be mitigated by imposing a constraint to preserve the total arc length of the element surface. The variation in arc length from each interior node j can be calculated as,

$$\frac{\partial S}{\partial \Delta n_j} = (-x_{j-1} + 2x_j - x_{j+1})\, n_x + (-y_{j-1} + 2y_j - y_{j+1})\, n_y + (-z_{j-1} + 2z_j - z_{j+1})\, n_z \tag{5}$$

At the endpoints the equivalent formula consists of one-sided differences; however, these are typically not needed due to other constraints being imposed. This introduces one additional equation,

$$\sum_{1}^{N} \frac{\partial S}{\partial \Delta n_j} \Delta n_j = 0 \tag{6}$$

into the overconstrained system. Note that Eq. 5 is based on a continuous derivative while Δn_j is discrete. Therefore, the arc length only approximately remains fixed. This could be made exact through the use of subiterations, but this has not been found necessary for practical cases.

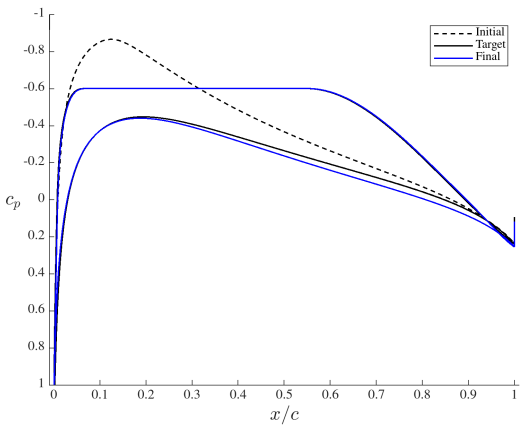
3. Results

The method was implemented in a program using MATLAB which imports solution data and the mesh from OVERFLOW 2.4b. This allowed for the calculated perturbations to be directly applied to the surface of the airfoil or wing. These displacements were also applied to points extending off the surface to mitigate excessively skewed grid cells and maintain positive cell volumes. Since the grid does not need to be regenerated, the CFD simulation can be restarted from the previous design, significantly decreasing simulation costs.

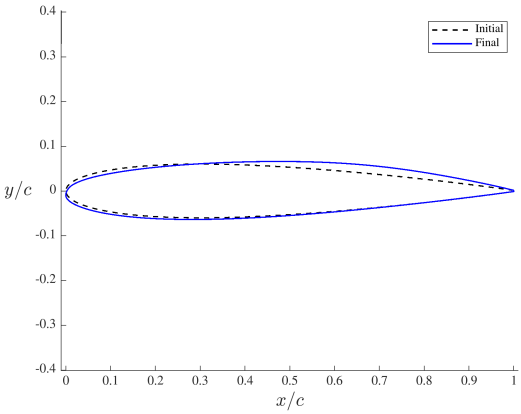
The following sections discuss the application of the method to various airfoils test cases and a wing test case. All simulations were run using the Spalart-Allmaras turbulence model [17]. Calculations were primarily done as fully turbulent despite the application being natural-laminar-flow airfoils. The reason for this is two-fold. First, transition can be sensitive to small perturbations in the airfoil shape, leading to poor convergence on a design. Second, the transition location is known to introduce a small perturbation in the pressure distribution, and this may inadvertently put a bump/dip in the surface due to the inverse design.

3.1 Single-Point, Single-Element Airfoil Design

To demonstrate the single-point design capabilities of method, an NACA 0012 airfoil test case at a Mach number of 0.7, Reynolds number of 6 million, and an angle of attack of 1° was used. The initial pressure distribution, calculated by OVERFLOW, was modified following CATNLF design philosophy, where the upper surface pressure distribution now features a constant c_p section at a value of -0.6, shown in Fig. 2a. The lower surface remained unmodified, but was still applied as a target pressure distribution. After 25 design iterations, the upper surface converged to the designated target distribution, while the lower surface deviated slightly from the target. The summation constraint was not used, instead the leading edge point of the airfoil was fixed to prevent excessive changes at the leading edge. After the design, the maximum thickness increased to 12.6% and shifted aft from 30%-chord to 36.6%-chord.



(a) Initial, target, and final pressure coefficient distributions.



(b) Initial and resulting airfoils from single point airfoil design.

Figure 2 – Initial and final pressure and airfoil distributions for single-point, single-element case.

3.2 Multipoint, Single-Element Airfoil Design

A second flight condtion was added to the previous test case to demonstrate the simultaneous, multipoint, modification of an airfoil at different flight conditions. To contrast the high speed cruise case, a low speed case at a Mach number of 0.2, Reynolds number of 6 million, and an angle of attack of 5°

was chosen. The pressure peak on the lower surface was decreased, shown in Fig. 3. This served as the target for the lower surface, while the previous test case governed the upper surface. Both flight conditions were stimulated and input into the design program simultaneously.

The summation constraint was applied to points residing before about 1%-chord. Correspondingly, the coefficient B was decreased to 0.22 and points along the thick trailing edge were fixed to prevent movement. After 58 design iterations, the pressure distributions showed good agreement with target for the upper and lower surface.

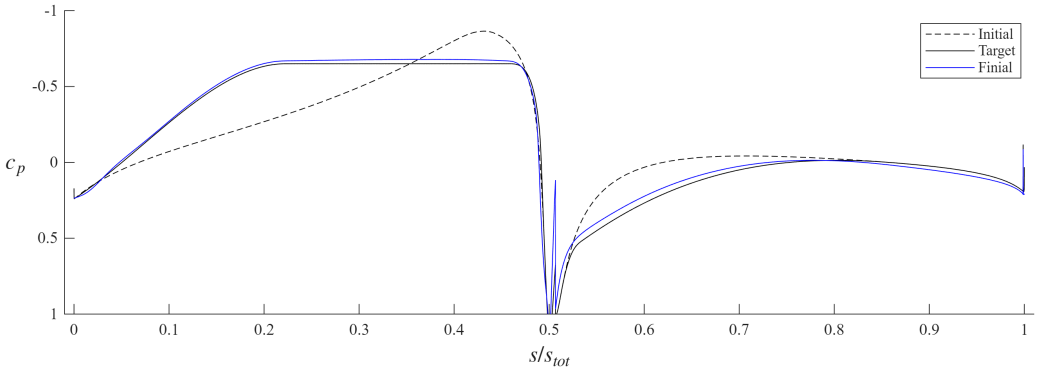


Figure 3 – Resulting pressure distribution from multipoint inverse design.

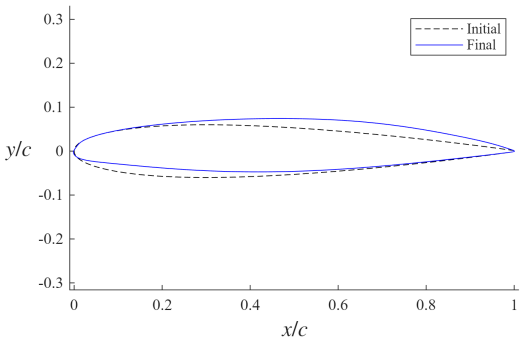


Figure 4 – Resulting airfoil from multipoint design.

3.3 Multipoint Slotted, Natural-Laminar-Flow Airfoil Design

A base slotted, natural-laminar-flow airfoil was simultaneously optimized at three flight conditions to demonstrate the use of a third flight condition. The cruise condition was set at a mach number of 0.747 and a Reynolds number of 8.5 million. The target pressure distribution for this flight condition was again inspired by the CATNLF design philosophy, with a constant c_p region ranging from 6%-chord to 60%-chord on the upper surface. The value of this constant c_p region, also referred to as rooftop, was set to -0.65, approximating the average c_p value in the rooftop region of the initial airfoil. At the end of this rooftop region, the pressure was set to recover linearly to the original trailing edge pressure. A superellipse was used to blend the leading-edge favorable pressure gradient region of the airfoil into the rooftop. The characteristic extremely favorable pressure gradient found on CATNLF airfoils is not present. This is to allow enough arclength for the specification of a low-speed, high-lift case. If this gradient is too favorable, the low-speed region would encroach upon the rooftop.

The low-speed, high-lift flight condition was set at a Mach number of 0.2, with same Reynolds number of the previous flight condition. The aim of this flight condition was to suppress the pressure spike at high angles of attack, therefore improving the maximum lift coefficient. A lift coefficient of 1.2 was selected and a minium c_p value -4.5 was imposed. Regions of the airfoil with a c_p value below the cutoff, were set to target a value of -4.5.

The final flight condition, named high-speed dash, was set at a freestream mach number of 0.747 with the same Reynolds number. This case was set at a c_l of 0 and used to smooth pressure oscillations found on the lower surface near the leading edge.

The constant B in Eq. 1 was set to 0.3. For the boundary conditions, Eq. 4 was applied to points residing before 3 percent of normalized chord of the airfoil with a weight of 1000 being used. The slot was fixed, as this region is sensitive to changes, as well as the entire aft element of the airfoil.

The targets and results of the inverse design are shown in Fig. 5. After 57 design iterations, the cruise case matched well with the prescribed target distribution. The high lift case, on the other hand, did not attain the targeted pressure. Convergence was hindered by the leading edge constraint, which effectively stiffens the system of equations. However, this deviation is acceptable, as strictly enforcing the target here would negatively impact performance at other flight conditions.

Near the leading edge, the high-speed dash case converged well and completely eliminated the oscillation. Moving aft along the fore element, however, the pressure distribution begins to deviate from the target due to the stronger localized influence of the fixed slot constraint.

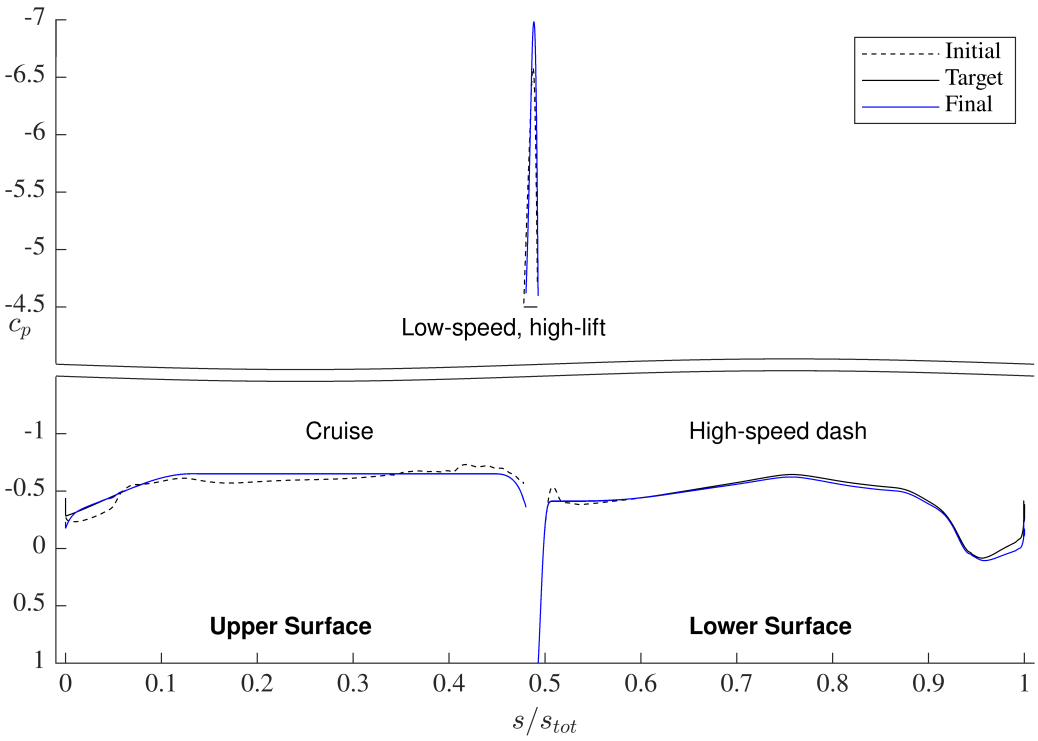


Figure 5 – Initial, target, and final pressure distributions

The resulting airfoil is shown in Fig. 6. Overall, the thickness remained roughly constant, with the max thickness increasing slightly from 11.71% to 11.88%. The location of max thickness shifting aftward, from 44.49%-chord to 44.78%-chord.

To compare the performance between the initial and the final airfoil, a c_l sweep was performed in MSES at a Mach number of 0.747 and a Reynolds number of 8.5×10^6. The redesigned airfoil shows a substantial improvement over the original airfoil.

3.4 Slotted, Natural-Laminar Flow Airfoil Design with Stronger Shock

A trait of the previous examples is that, while they are transonic, they do not have strong shockwaves. This is not a limitation of the method. Rather, cases with strong shockwaves can be treated by relaxing the specification downstream of the anticipated shock location. It could be left to "float" (i.e.,

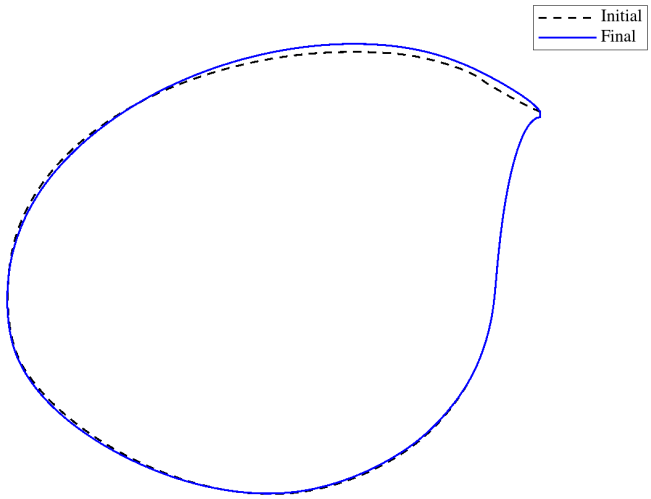


Figure 6 – Initial and final SNLF fore-element geometries after multipoint inverse (re-)design

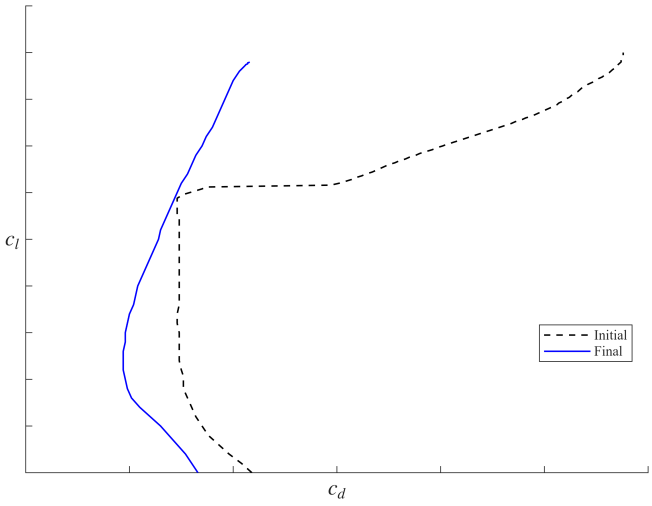


Figure 7 – Comparison of drag polars for initial and final SNLF airfoil after multipoint inverse (re-)design

$\Delta c_p = 0$ in this region), or that segment could be specified for a condition where that region is fully subsonic. An example of this is included below for a slotted, natural-laminar-flow airfoil at $M = 0.75$, $c_l = 0.50$, and $Re = 6 \times 10^6$. Here, a linear c_p ramp with $dc_p/dx = -0.05$ was specified over the range $x/c = [0.02, 0.65]$. The lower-surface design point was the same Mach number but $c_l = 0.2$ with a simple smoothing applied to the pressures after each design iteration. The final airfoil produces the desired ramp behavior at the correct lift coefficient, confirming the efficacy of the strategy for strong shocks. Note that this case used transitional RANS rather than fully turbulent at the primary design point to ensure correct boundary-layer development.

3.5 Single-Point, Single-Element Wing Design

For a three-dimensional test case, a simple wing and body configuration was created on approximately the same scale as a business jet, shown in Fig. 10a. It features a span of 720 inches and a body length of 600 inches, which consists of a 6:1 prolate spheroid. The baseline wing was generated from CRM-NLF airfoils with a 20-degree sweep. The root chord is 124.18 inches with a tip chord of 31.5 inches. This test case was run with freestream Mach number of 0.78 and a Reynolds number of 73,500 per inch.

Five spanwise stations were chosen and the pressure distributions were modified to include a rooftop at $c_p = -0.6$ starting at 3%-chord and ending at 55%-chord on the upper surface. The lower surface target distribution was modified to eliminate the shock. The airfoil sections were lofted between the

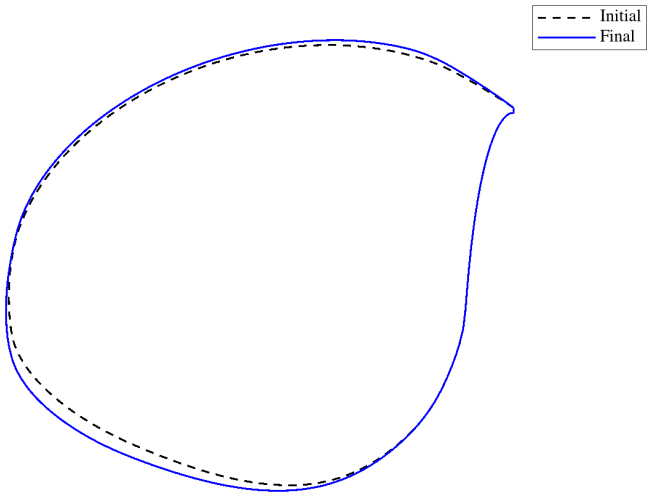


Figure 8 – Initial and final SNLF fore-element geometries after upper-surface ramp specification.

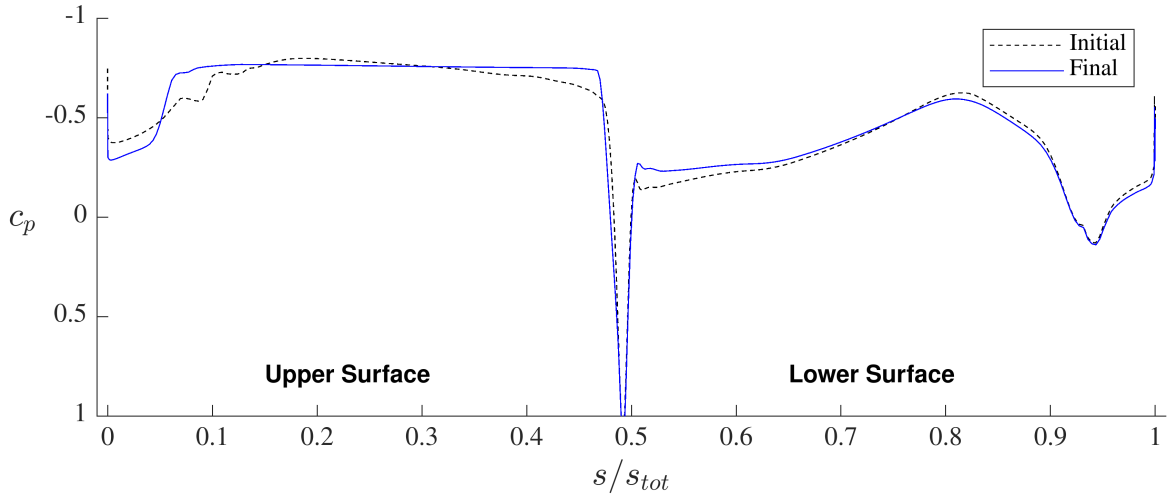
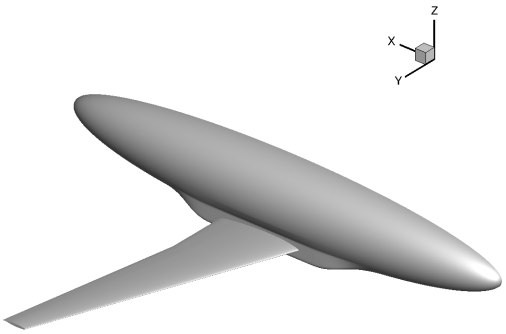


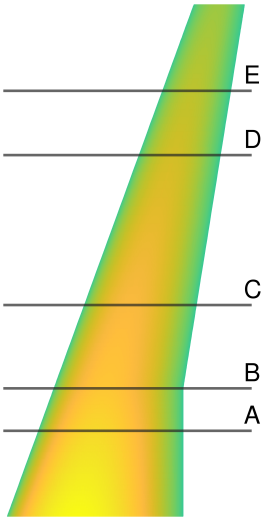
Figure 9 – Initial and final pressure distributions after upper-surface ramp specification.

spanwise stations. Inboard and outboard of station A and E, respectively, the regions were blended into the original geometry. To avoid infringing on the overset surface mesh, the tip and root of the wing were not modified. Points along the thick trailing edge and the leading edge point of each airfoil station were fixed.

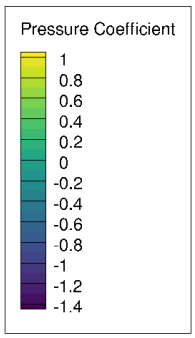
After 130 design iterations, the rooftop for each spanwise location was matched well, while the lower surface deviated from the prescribed target. However, both the shocks from the upper and the lower surface were eliminated. Fig. 11 shows pressure contours on the upper surface of the wing, although the regions between the stations were lofted linearly, there is no visible discontinuity in contour.

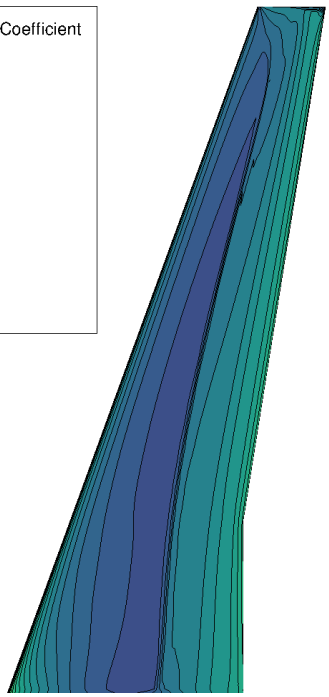


(a) Wing body test case

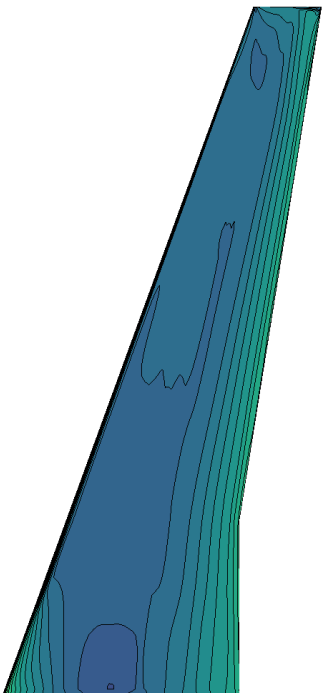


(b) Spanwise inverse design stations



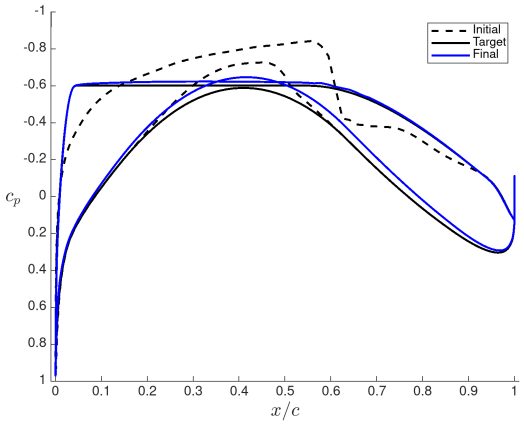


(a) Initial wing C_p contours

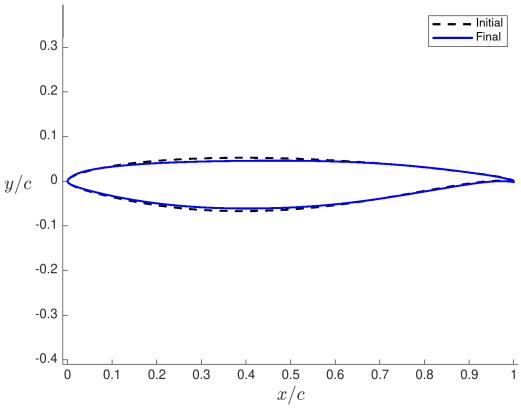


(b) Final iteration wing C_p contours

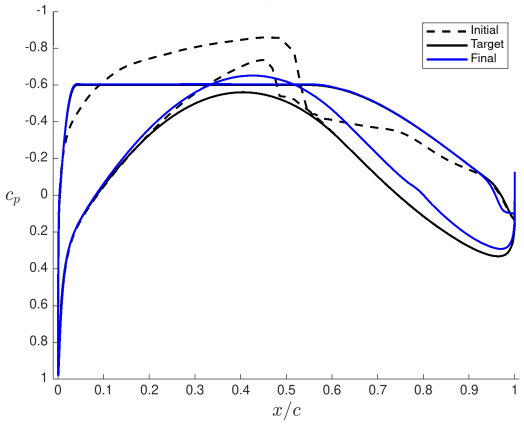
Figure 11 – Upper surface C_p contours before and after 130 iterations



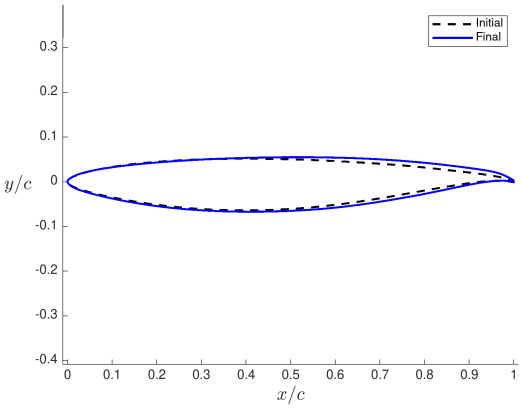
(a) Station A C_p distributions



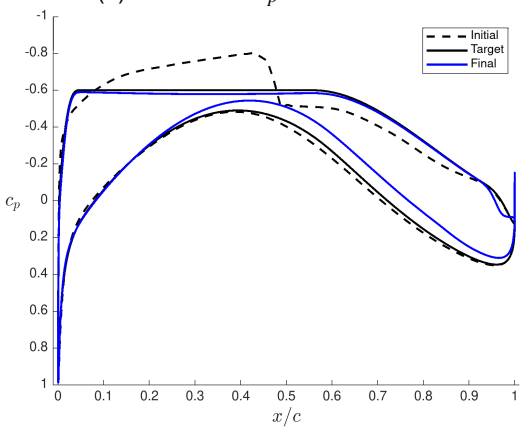
(b) Station A airfoils



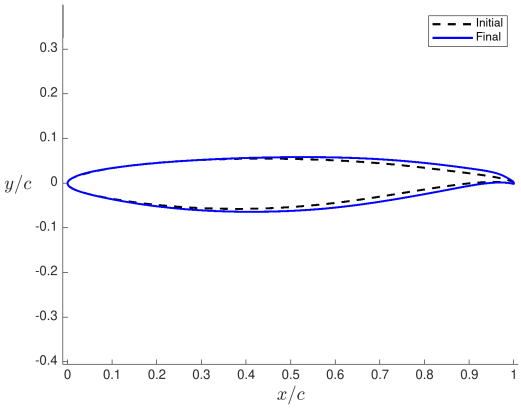
(c) Station C C_p distributions



(d) Station C airfoils



(e) Station E C_p distributions

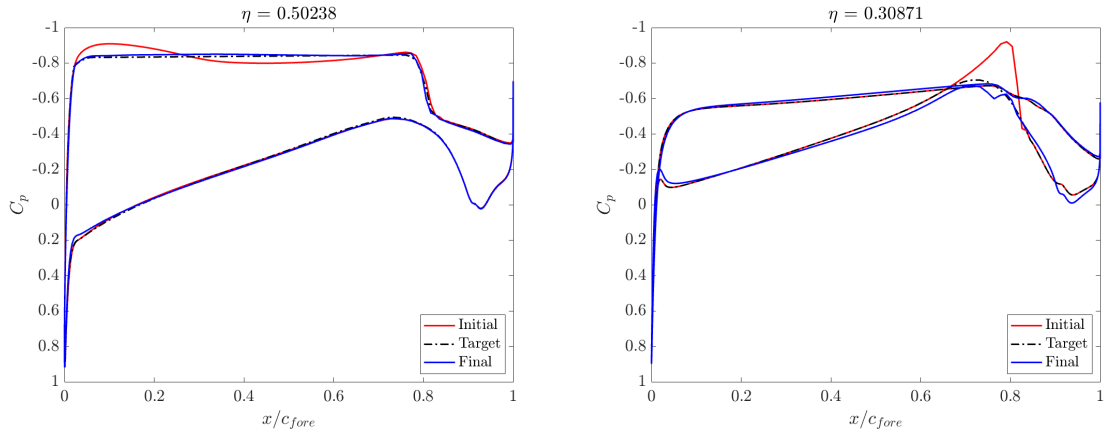


(f) Station E airfoils

Figure 12 – C_p distributions and airfoil shapes at the start and end of the inverse design for multiple spanwise stations.

3.6 Multipoint, Slotted, Natural-Laminar-Flow Wing

The final example is for a three-dimensional, SNLF wing redesign for conditions representative of a light business jet. Transitional RANS calculations were performed to ensure correct boundary-layer growth. Multipoint design of the fore element was conducted for two design points. The first design point was selected to be a heavy, higher-altitude, start-of-cruise condition at $M = 0.78$ to drive the upper-surface design. The second design point was selected to be a light, lower-altitude overspeed condition. This point was chosen based on analysis of the initial design, which showed the formation of a strong lower-surface shockwave. The design targets were selected to imposed a rooftop pressure distribution at cruise and remove the overspeed shockwave. The initial, target, and final pressure distributions are shown in Fig. 13. The design process was found to be successful and gave a very good approximation of the target pressure distributions.



(a) Midspan station at cruise design point. (b) Inboard station at overspeed design point.

Figure 13 – Initial, target, and final pressure coefficient distributions of SNLF fore element.

4. Conclusion

A method was presented for performing three-dimensional inverse design of slotted, natural-laminar-flow wings. The method is based on the CDISC methodology of Campbell and Smith [14], which uses the pressure-curvature relationship to determine the surface updates and is generally applicable in three dimensions unlike many other tools. The improvements made include a more sophisticated mathematical formulation based on Newton-Raphson iteration that allows the target pressure distribution to be prescribed in a discontinuous manner for multiple design points. Geometric constraints are handled by overconstraining the system of equations and solving using least squares. This allows the effect of the constraint to be distributed more evenly along the surface and mitigate potential discontinuities in the surface curvature. The method was applied to various test cases, including both single-element and multielement airfoils and both single- and multielement wings, confirming its efficacy.

Ongoing work involves maturing the tool's codebase, converting it from MATLAB to Python for better portability, and increasing its modularity. Future work includes coupling the tool with a Falkner-Skan-Cooke boundary-layer solver to allow Tollmien-Schlichtin and crossflow transition margins to be included as part of the design specifications. Other ongoing work is exploring the use of machine learning to improve the estimate of $dc_p/d\kappa$, which is anticipated to greatly improve its convergence capabilities in general scenarios.

5. Contact Author Email Address

Mailto: Andrew Heletkanycz avh5950@psu.edu

6. Copyright Statement

The authors confirm that they, and/or their company or organization, hold copyright on all of the original material included in this paper. The authors also confirm that they have obtained permission, from the copyright holder of any third party material included in this paper, to publish it as part of their paper. The authors confirm that they give permission, or have obtained permission from the copyright holder of this paper, for the publication and distribution of this paper as part of the ICAS proceedings or as individual off-prints from the proceedings.

Acknowledgments

Development of the multipoint inverse design tool was supported through funding from the United States Federal Aviation Administration under Grant Agreement No. 69A3352540041 titled "Wind Tunnel Testing of a Transonic Aircraft with a Fully Integrated, Slotted Natural Laminar Flow (SNLF) Wing" through Otto Aerospace. Any opinions, findings, and conclusions or recommendations ex-

pressed in this material are those of the author(s) and do not necessarily reflect the views of the FAA.

References

[1] Marty K. Bradley and Christopher K. Droney. Subsonic Ultra Green Aircraft Research Phase II: N+4 Advanced Concept Development. Technical Report NF1676L-14434, May 2012. NTRS Author Affiliations: Boeing Research and Technology NTRS Document ID: 20120009038 NTRS Research Center: Langley Research Center (LaRC).

[2] E. M. Greitzer, P. A. Bonnefoy, E. DelaRosaBlanco, C. S. Dorbian, M. Drela, D. K. Hall, R. J. Hansman, J. I. Hileman, R. H. Liebeck, J. Levegren, P. Mody, J. A. Pertuze, S. Sato, Z. S. Spakovszky, C. S. Tan, J. S. Hollman, J. E. Duda, N. Fitzgerald, J. Houghton, J. L. Kerrebrock, G. F. Kiwada, D. Kordonowy, J. C. Parrish, J. Tylko, and E. A. Wen. N+3 Aircraft Concept Designs and Trade Studies. Technical Report E-17419-1, December 2010. NTRS Author Affiliations: Massachusetts Inst. of Tech., Aurora Flight Sciences, Inc. NTRS Document ID: 20100042401 NTRS Research Center: Glenn Research Center (GRC).

[3] Madelyn Focaracci, Lauren Wolfe, Daniel Gil-Prieto, Georgi K. Hristov, Deborah Neuman, Francesco Giannini, Aaron Kutzmann, Martha Neubauer, Jose Martinez, Neal Quinn, and Zachary Hoisington. *AACES 2050 Phase I: Aurora Flight SciencesStudy Overview*.

[4] Ronald D. Joslin. Overview of Laminar Flow Control, October 1998. NTRS Author Affiliations: NASA Langley Research Center NTRS Report/Patent Number: NASA/TP-1998-208705 NTRS Document ID: 19980232017 NTRS Research Center: Langley Research Center (LaRC).

[5] Edward B. White William S. Saric, Helen L. Reed. Stability and transition of three-dimensional boundary layers. *Annual Review of Fluid Mechanics*, 35(1):413–440, 2003.

[6] Michelle N. Lynde, Richard L. Campbell, Brett R. Hiller, and Lewis R. Owens. Design of a crossflow attenuated natural laminar flow flight test article. 2021.

[7] Dan M. Somers. Laminar-flow airfoil. In *US Patent 6,905,092 B2*, June 14, 2005.

[8] James G. Coder and Dan M. Somers. Design of a slotted, natural-laminar-flow airfoil for commercial transport applications. *Aerospace Science and Technology*, 106:106217, 2020.

[9] James G. Coder. Transonic wind-tunnel testing of a slotted, natural-laminar-flow wing at full-scale conditions. *CEAS Aeronautical Journal*, 2026.

[10] Brett R. Hiller, Richard L. Campbell, and Michelle N. Banchy. Cruise slotted wing design with natural laminar flow for transonic commercial transport aircraft. In *AIAA SciTech 2025 Forum*, Orlando, FL, January 2025. AIAA Paper 2025-0244.

[11] Richard Eppler and Dan M. Somers. A computer program for the design and analysis of low-speed airfoils. Technical Report NASA TM-80210, National Aeronautics and Space Administration, Washington, D.C., USA, August 1980. Prepared at Langley Research Center.

[12] Michael S. Selig and Mark D. Maughmer. Generalized multipoint inverse airfoil design. *AIAA Journal*, 30(11):2618–2625, 1992.

[13] Mark Drela. *MSES User's Guide*. Massachusetts Institute of Technology, Cambridge, MA, 2007. Accessed: May 11, 2026.

[14] Richard Campbell and Leigh Smith. A hybrid algorithm for transonic airfoil and wing design. In *5th Applied Aerodynamics Conference*, Fluid Dynamics and Co-located Conferences. American Institute of Aeronautics and Astronautics, August 1987.

[15] Richard L. Campbell, Michelle N. Banchy, and Brett R. Hiller. *History and Status of the CDISC Aerodynamic Design Method*.

[16] Michelle N. Lynde, Richard L. Campbell, Brett R. Hiller, and Lewis R. Owens. Design of a crossflow attenuated natural laminar flow flight test article. In *AIAA Scitech 2021 Forum*, page 0173, Reston, VA, 2021. American Institute of Aeronautics and Astronautics.

[17] P. R. Spalart and S. R. Allmaras. A one-equation turbulence model for aerodynamic flows. *Recherche Aerospatiale*, No. 1, 1994, pp. 5-21.